Shape memory nanocomposite of poly(L-lactic acid)/graphene nanoplatelets triggered by infrared light and thermal heating

eXPRESS Polymer Letters Vol.10, No.4 (2016) 349–359
Available online at www.expresspolymlett.com
DOI: 10.3144/expresspolymlett.2016.32

Shape memory nanocomposite of poly(*L*-lactic acid)/graphene nanoplatelets triggered by infrared light and thermal heating

S. Lashgari[1,2], *M. Karrabi*[1*], *I. Ghasemi*[1], *H. Azizi*[1] , *M. Messori*[2], *K. Paderni*[2]

[1]Iran Polymer and Petrochemical Institute (IPPI), 14965/115, Tehran, Iran
[2]Department of Engineering 'Enzo Ferrari', University of Modena and Reggio Emilia, 41125 Modena, Italy

Received 3 September 2015; accepted in revised form 16 November 2015

Abstract. In this study, the effect of graphene nanoplatelets (GNPs) on the shape memory properties of poly(*L*-lactic acid) (PLLA) was studied. In addition to thermal activation, the possibility of infrared actuating of thermo-responsive shape memory PLLA/GNPs nanocomposite was investigated. The incorporated GNPs were expected to absorb infrared wave's energy and activate shape memory PLLA/GNPs. Different techniques such as differential scanning calorimetry (DSC), wide-angle X-ray diffraction (WAXD), field emission gun scanning electron microscope (FEG-SEM) and dynamic mechanical thermal analysis (DMTA) were used to characterize samples. DSC and WAXD results indicated that GNPs augmented crystallinity due to nucleating effect of graphene particles. GNPs improved both thermal and infrared activating shape memory properties along with faster response. Pure shape memory PLLA was slightly responsive to infrared light and its infrared actuated shape recovery ratio was 86% which increased to more than 95% with loading of GNPs. Drastic improvement in the crystallinity was obtained in nanocomposites with lower GNPs contents (0.5 and 1 wt%) due to finer dispersion of graphene which resulted in more prominent mechanical and shape memory properties enhancement. Infrared activated shape memory PLLA/GNPs nanocomposites can be developed for wireless remote shape control of smart medical and bio-systems.

Keywords: *smart polymers, infrared triggering, nanocomposites, poly(L-lactic acid), graphene*

1. Introduction

Shape memory polymers (SMPs) are a class of smart materials which can recover their primary shape after being deformed to temporary shape [1]. Nowadays these polymers have attracted tremendous attention owing to wide potential applications being expected for these materials in different industries. Smart textiles [2, 3], intelligent medical devices [4, 5] and heat shrinkable films [6] are only some current usages of these polymers. Many scientific studies on this materials are being done and several articles and reviews have been published on this area [1, 7–11]. The stimuli used for activation of SMPs are basically classified into three types; heat (thermo-responsive), light (photo-responsive) and chemical (chemo-responsive) [12]. Thermo- and chemo-responsive shape memory effects (SME) are intrinsic feature of most polymers and are not special characteristic of some special polymers [12]. Thermo-responsive SME is the most popular case and includes both heating and cooling [13]. Heating can be applied directly or non-directly. Stimuli such as electrical resistive heating [14], magnetic field [15], infrared and UV heating light [16, 17] are examples of non-direct heating. Although there are various actuation methods for activating SMPs, but most of shape memory polymers are only able to be actuated through direct heating [18] and triggering with other stimulus is more complex. Nevertheless, many new actuation methods enable remote controlling of SMPs which expand their application in the areas that were impossible for traditionally thermally

*Corresponding author, e-mail: m.karabi@ippi.ac.ir

responsive SMPs. Therefore, SMPs being responsive to other types of stimuli have been gaining increasing interest over the recent years. SMPs based on biopolymers are in spotlight more than the other polymers due to their potential usage in pharmaceutical and medical devices such as surgical sutures, vascular stents, shaping tissue and controlled drug delivery systems [19–23]. Among them poly(lactic acid) (PLA) is one of the most promising biopolymers derived from 100% renewable resources such as corn, tapioca roots and sugarcane which can be readily degraded to lactic acid through hydrolysis [24]. Therefore, it has more extensive application in the medical industry compared to other bio-polymers [25]. Due to its bio properties and intrinsic shape memory abilities, this polymer has attracted interests of researchers and industries in this field and its shape memory properties have been studied by some researchers until now [23, 24, 26–32] However, most of mentioned studies have focused on thermal actuation and researches on multi-stimuli poly(lactic acid) shape memory are still lacking. Paakinahoet and coworkers [18, 33] reported water induced poly(*D*,*L*-lactide) shape memory polymer which is able to recover its shape at the aqueous environment at body temperature. Zhang *et al*. [22], and Zheng *et al*. [34] produced PLLA-Fe_3O_4 shape memory composite with thermal and magnetic field responsiveness.

Actuation by stimuli other than heat needs special functionalities in the polymer which are acquired through different ways. One of the facile and effective routes is the incorporation of special fillers into polymeric systems. Among the fillers, graphene is one of the most important carbonaceous fillers which has a range of extraordinary mechanical, thermal and electrical properties [35, 36] attracted a lot of attention in the polymeric systems. Introduction of graphene into polymers confers novel properties to shape memory composites including quicker response to thermal activation and the capability of responding to other stimuli such as infrared (IR) light, electricity, magnetic and others. These unique properties of graphene have been used to produce different multi-stimuli responsive SMPs. Infrared light actuated SMPs are a class of these materials and some studies have been done in this regard [17, 37, 38]. Kashif *et al*. [37] have produced shape memory polyolefin elastomer/modified graphene nanocomposites responding to infrared light with healing properties. Feng *et al*. [38] have prepared IR actuated shape memory polyurethane with the aid of reduced graphene oxide and carbon nanotube hybrids. Park and Kim [17] have studied on the semi-crystalline polyurethane/graphene shape memory nanocomposite system responding to infrared light. Tang *et al*. [39] have added graphene to polyester/carbon nanofibers composite to improve its capability in responding to various stimuli. However, literature reporting on the graphene based biodegradable SMPs respondent to infrared light is still limited.

Herein, we reported one type of graphene-containing shape memory PLLA which is capable of responding to direct thermal heating and infrared light. The effect of graphene on crystallinity and its correlation with shape memory and thermomechanical properties are studied. To the best of our knowledge, although some studies have been done on the PLLA/graphene system [40–44] until now, but this system is not already reported and described in the literature in terms of shape memory behavior. On the other hand, the infrared triggering of shape memory PLLA has not been investigated so far and our experimental evidence regarding infrared sensitivity of PLLA/graphene composites can be helpful for designing remote controlling shape memory devices.

2. Experimental

2.1. Materials

Poly(*L*-lactic acid) PLLA 3251D (1.4 mol% *D*-lactic acid, 98.6 mol% *L*-lactic acid content, average molecular weight of 90~120 kg/mol) was obtained from Natureworks (USA). Graphene nanoplatelets GNPs (grade C-750, the average thickness of 1–5 nm, length of less than 2 μm and superficial area 750 m^2/g) were purchased from XG Sciences (Lansing, USA). Chloroform was supplied by Sigma-Aldrich.

2.2. Sample preparation

At first, PLLA and GNPs were dried in a vacuum oven at 80 °C for 12 h to remove moisture completely. PLLA/GNPs nanocomposite samples were prepared by solution casting at 0.5, 1, 2, 4 and 6 wt% loading of GNPs. Desired amounts of the dried GNPs were added to chloroform (75 mL) and stirred at room temperature for 1 day with a magnetic stirrer, then 75 mL of PLLA solution (200 mg/mL) was added to the suspension, after that, it was put in the ultrasonic bath (Elma T460) for 15 minutes, at last, final products were poured into Petri dish and left for

1 day at room temperature to allow chloroform evaporation following by drying in vacuum oven at 60 °C for 24 h for complete evaporation of solvent. After drying, the films were pressed in an electrically-heated hydraulic press at 210 °C under 1000 kPa pressure for 3 min after 5 min preheating and then quickly cooled to room temperature by circulating cold water. The samples were denoted according to GNPs [wt%] loadings as PLLA-GNP0.5, PLLA-GNP1, PLLA-GNP2, PLLA-GNP4 and PLLA-GNP6 with 0.5, 1, 2, 4 and 6 wt% of GNPs, respectively.

2.3. Characterization

2.3.1. Morphology

Fractured surfaces of the PLLA/GNPs nanocomposites were observed using a high-resolution field emission gun SEM microscope (FEG-SEM, Nova NanoSEM 450, FEI of USA). The samples were fractured in liquid nitrogen prior to FEG-SEM imaging.

2.3.2. DSC and WAXD

To study thermal properties of specimens and effect of graphene on these properties, differential scanning calorimetry (DSC) (TA Instruments DSC 2010, New Castle, DE, USA) analysis was carried out at nitrogen atmosphere. Thermal history of specimens was erased through a first heating scan from 0 to 250 °C at a heating rate of 10 °C/min, then cooled to the room temperature at a cooling rate of 10 °C/min, followed by a third scan at the same heating rate to 250 °C. The mid-point of the start and end of the transition in DSC curves was taken as the T_g^{DSC} value. The glass transition temperature (T_g^{DSC}), cold crystallization temperature (T_{cc}), cold crystallization enthalpy (ΔH_{cc}), melting temperature (T_m) and melting enthalpy (ΔH_m) were determined from the second heating curve. The degree of crystallization (χ_c) was obtained using the following Equation (1):

$$\chi_c[\,\%\,] = \frac{\Delta H_m - \Delta H_{cc}}{\Delta H_m^0(1-\varphi_f)} \cdot 100 \tag{1}$$

where ΔH and ΔH_{cc} are the melting enthalpy and the cold crystallization enthalpy of test sample respectively, ΔH_m^0 is the melting enthalpy of the 100% crystalline PLLA (93.0 J/g [45]) and φ_f is the weight percentage of filler.

For a better analysis of crystallinity, wide angle X-ray diffraction (WAXD) test was done on samples using Panalytical X' Pert Pro instrument. Test scanning rate was 5°/min at 40 kV and 100 mA with Cu-Kα1 irradiation (λ = 1.54 Å) in the range of 10~60°.

2.3.3. Shape memory performance

Shape memory performances of samples were investigated by two actuation methods, direct heating, and infrared light. Programming of temporary shape in direct heating actuation was carried out through a four-stage thermo-mechanical cycle by means of a dynamic mechanical thermal analysis instrument (DMA Q800, TA Instruments, New Castle, DE, USA). Rectangular strips of samples were programmed under fixed-strain condition according to later steps: (1) deforming the specimen at T_H = 75 °C under a loading ramp at 10 MPa·min^{-1} up to 100% strain, (2) cooling the specimen to T_L = 0 °C instantly by keeping the attained strain constant, (3) maintaining the sample at T_L for 30 min after removal the load, and (4) raising the temperature from T_L to T_H then maintaining at the latter for 30 min. Under these conditions, shape fixity rate (R_f) and shape recovery rate (R_r) are defined according to following Equations (2) and (3) [46]:

$$R_f(N) = \frac{\varepsilon_u(N)}{\varepsilon_m} \cdot 100\,\% \tag{2}$$

$$R_r(N) = \frac{\varepsilon_m - \varepsilon_p(N)}{\varepsilon_m - \varepsilon_p(N-1)} \cdot 100\,\% \tag{3}$$

where $\varepsilon_u(N)$ is the tensile strain after unloading at T_L in the N^{th} cycle (N), ε_m is maximum strain. $\varepsilon_p(N)$ and $\varepsilon_p(N-1)$ are the unrecovered strains after heating the sample to T_H in the N^{th} cycle and previous one, respectively.

Bending test [47, 48] was utilized to study the feasibility of IR actuation of SMP composites. Rectangular strips of PLLA/GNPs nanocomposites (60 mm× 5 mm×1 mm) were deformed into U-like shape at 75 °C followed by rapid cooling with liquid nitrogen to fix deformation. An infrared (IR) lamp (Philips, 150 W) was used as the IR activation light source. The distance between lamp and specimen was 25 cm. The power density to samples was around 20 mW/cm^2 measured by a light density meter. The recovery ratio (R_r) was calculated according to Equation (4), in which θ is the returned angle of the strip from temporary U-like shape to the original one. In all cases, more than three samples were tested, from which the mean and standard deviation were calcu-

lated. An infrared video camera (InfRec Thermo GEAR, G120) was used in our study to monitor the temperature distribution and shape recovery behavior simultaneously (Equations (4)):

$$R_r = \frac{\theta}{180^\circ} \cdot 100\% \quad (0^\circ < \theta < 180^\circ) \tag{4}$$

2.3.4. Dynamic mechanical thermal analysis (DMTA)

Thermomechanical properties of the samples were measured by means of DMA Q800 (TA Instruments, New Castle, DE, USA) using rectangular strips (overall length: 25 mm; length between grips: 8 mm; width: about 5 mm, thickness: 1 mm) operating in the tensile mode at an oscillation frequency of 1 Hz with a static force of 10 mN and a oscillation strain of 0.05%. The samples were measured over a temperature range from room temperature to 160 °C at a heating rate of 5 °C/min.

3. Results and discussion

3.1. Microstructure

Figure 1 shows the FEG-SEM micrographs of fractured surface of PLLA/graphene with 1 and 4 wt% of GNPs at the magnification of 12 000×. As can be seen, graphene nanoplatelets exhibited fine dispersion and uniform distribution in the matrix with a little aggregation in the latter sample (squares in Figure 1b) due to higher filler content. Therefore, it seems that better thermal and mechanical properties can be attained in nanocomposites with lower GNPs content. The homogenous distribution of graphene in the matrix is associated to the relatively good interaction of PLLA and GNPs resulting in uniform infrared absorption in the shape memory test which is investigated further.

3.2. Thermal and crystallinity analysis

Glass transition temperature (T_g) and crystallinity status are two important factors in T_g based semi-crystalline SMPs which are considered as the switching temperature and fixed phase of SMPs, respectively. So it is important to investigate the effect of graphene on the T_g and crystallinity of PLLA prior to shape memory studying. Figure 2 depicts cooling thermograms and 2nd heating thermograms of DSC scans and the detailed data derived from them are summarized in Table 1. As can be seen, T_g values of PLLA/ GNPs composites are slightly increased with addition of GNPs compared to pure PLLA. This may be attributed to chain mobility restriction caused by GNPs particles resulting in higher T_g temperatures. However, owing to small shifting in glass transition temperature, the switching temperature of all samples in shape memory tests can be considered identical. The peaks specified in the cooling thermograms are related to the crystallization temperature (T_c) of specimens. As can be seen, at low graphene loading (0.5 and 1 wt%) nanocomposites, the T_c peak intensified drastically and shifted to higher temperatures compared to pure PLLA. This means that the incorporation of graphene into PLLA at low contents favored the formation of crystalline domains and enhanced crystallinity percentage (%X_c) which are presented in Table 1. Undoubtedly, this significant rise of crystallinity is associated to the nucleating effect of graphene which enhances the crystallization kinetic of PLLA and leads to the formation of more crys-

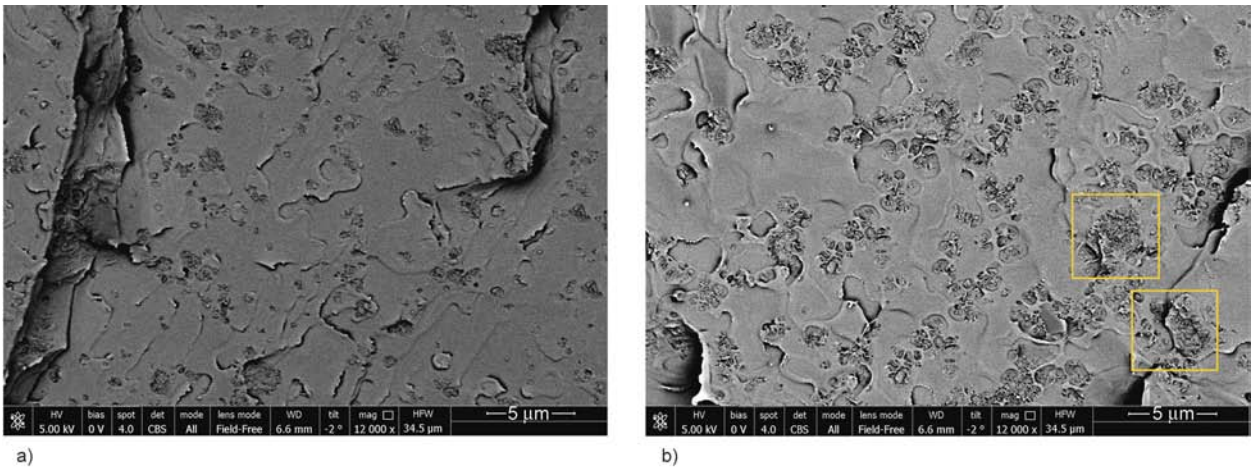

Figure 1. FEG-SEM images of (a) PLLA-GNP1 nanocomposite and (b) PLLA-GNP4 nanocomposite

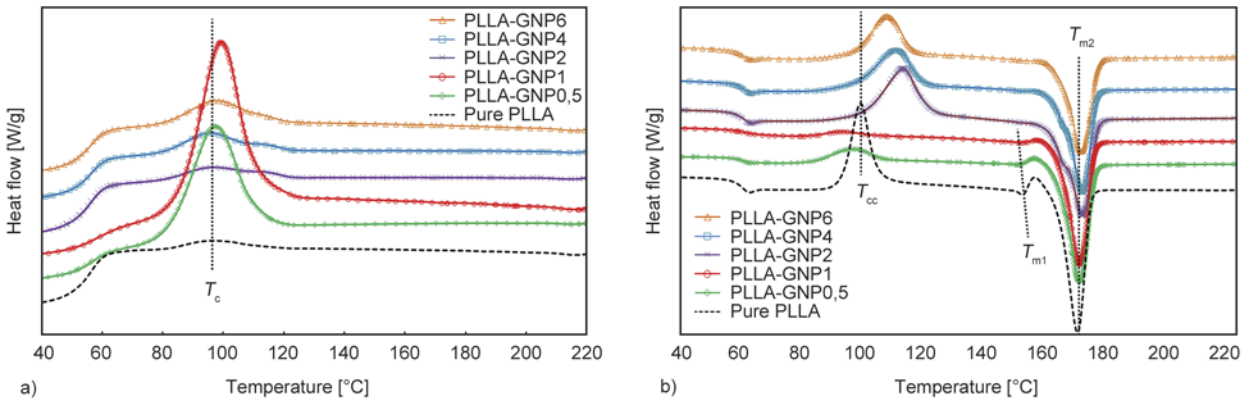

Figure 2. (a) cooling thermograms and (b) 2nd heating thermograms of pure PLLA and its nanocomposites with various loading of GNPs

Table 1. Thermal properties of PLLA and its composites derived from DSC analysis

Sample	DSC Data								
	%GNPs	T_g^{DSC}	T_{cc}	T_{m1}	T_{m2}	T_c	ΔH_{cc}	ΔH_m	$\%X_c$
Pure PLLA	0	59.9	98.4	150.9	168.6	96.0	41.2	49.3	8.7
PLLA-GNP0.5	0.5	61.3	96.2	149.6	169.2	97.2	13.4	47.5	36.8
PLLA-GNP1	1	61.0	92.9	150.1	169.3	99.2	6.9	44.7	41.1
PLLA-GNP2	2	60.1	112.2	162.8	170.3	95.9	32.0	40.5	9.4
PLLA-GNP4	4	60.5	110.0	–	170.1	95.3	32.3	39.3	7.8
PLLA-GNP6	6	60.0	104.5	–	169.2	97.8	32.1	39.8	8.8

tals. However, over 1 wt% graphene loading, T_c peaks shift back to lower temperatures and their intensity are decreased drastically. Meanwhile, their crystallinity percentage ($\%X_c$) are reduced to as low as pure PLLA in these samples. This is because, with the rise of graphene percentage, particles would be tending to aggregate as already illustrated in Figure 1. Therefore, although they act as the nucleating agent, but they would hinder chain mobility and depress the crystallinity at the same time. Following the changes in the crystallinity, addition of GNPs caused in shifting of cold crystallization temperature (T_{cc}) (Figure 2b) to lower temperatures at low graphene loadings (0.5 and 1 wt%) from 98.4 to 92.9 °C and shifting back to higher values as GNPs composition rises to 2 and higher wt% of GNPs . Therefore, few amounts of GNPs are seemed suitable for enhancement of crystallinity through providing nucleation sites.

Double melting point which is ascribed to melt-recrystallization mechanism or crystals with different structures or different degree of perfections [49] is observed in pure PLLA and nanocomposites. The sharp peak of T_{m1} in the pure PLLA may be related to melt re-crystallization of less perfect crystals formed during cold crystallization. However, presence of GNPs caused to decrease of this peak in the PLLA-GNP0.5 and PLLA-GNP1 due to their nucleating effect that leaded to faster crystallinity kinetics with the formation of more perfect crystals directly in the cooling process. As already mentioned, with increase of GNPs to more than 1 wt%, crystallinity percentage showed decreasing trend and melting peaks merged together and T_{m1} appeared as a step in main melting peak of PLLA-GNP2 and disappeared in the PLLA-GNP4 and PLLA-GNP6.

The disappearance of T_{m1} peak in the latter composites may correspond to their higher T_{cc} compared to pure PLLA which would result in the formation of more stable and perfect crystals during cold crystallization process due to enhancement of segment mobility at higher T_{cc} temperatures.

To gain more insight into crystallinity and effect of GNPs, WAXD analysis was carried out. Figure 3 exhibits the WAXD patterns of GNPs, pure PLLA, and its nanocomposites. The peak at $2\theta = 26.5°$ in GNPs is associated to the (002) diffraction peak of pristine graphene nanosheets. The GNPs peak is not observed in the composites containing of 0.5 and 1 wt% of graphene indicating a good exfoliation that was confirmed by FEG-SEM images (Figure 1a for PLLA-GNP1), however this peak appeared slightly (shown by arrow in Figure 3) beyond 2 wt% of GNPs loading (PLLA-GNP4 and PLLA-GNP6) which is related to the agglomerates that are not completely separated (as specified in Figure 1b for PLLA-

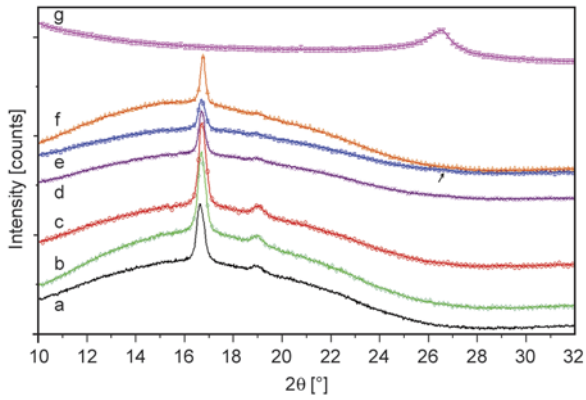

Figure 3. WAXD patterns of (a) pure PLLA, (b) PLLA-GNP0.5, (c) PLLA-GNP1, (d) PLLA-GNP2, (e) PLLA-GNP4, (f) PLLA-GNP6 and (g) GNPs

GNP4). The peaks around $2\theta = 16.7$ and 19° are ascribed to α crystals of PLLA [28]. These peaks are observed in all of nanocomposites suggesting the crystalline structure of PLLA is not changed with the incorporation of GNPs. The intensity of peaks increased enormously at low graphene loading (0.5 and 1 wt%). However, marginal changes are seen over 2 wt% GNPs fraction. These observations are in line with the DSC results and correspond to higher crystallinity percentage at lower GNPs content due to better dispersion and nucleating of graphene particles.

3.3. Thermo-mechanical analysis

Storage modulus (E') and damping factor ($\tan\delta$) diagrams of pure PLLA and its nanocomposites are shown in Figure 4. As expected, storage modulus of nanocomposites is enhanced below T_g compared to that of pure PLLA due to the reinforcing effect of GNPs particles. Moreover, as already has reported [50], in the nano-sized polymer composites, the size of fillers is similar to the size of polymer segments, so the thermomechanical behavior of polymer segments is more affected by the fillers which is considered as the friction interactions resulting to improved mechanical properties. However, the increasing is not in a monotonic trend and starts dropping beyond 4 wt%. This may be corresponding to the aggregates at the higher GNPs fractions (Figure 1b) lowering stiffening effect of graphene and leading to decrease of storage modulus. Meanwhile, as reported by Zhenge *et a*l. [32], higher glassy modulus will result in larger shape fixity in the cooling cycle and larger shape recovery in the heating process which is further corroborated by the shape memory results. The peaks of $\tan\delta$ curves are related to the glass transition temperatures (T_g^{DMTA}) of the samples. The T_g^{DMTA} of pure PLLA is ~80 °C and the addition of GNPs is caused to increase of T_g^{DMTA} due to the restriction effect of GNPs on the chain mobility of PLLA. The T_g obtained through DMTA is higher than the T_g acquired by DSC results. This is related to the difference of T_g definition in two techniques and also the heat transport hysteresis for larger scale samples in DMTA, while the DSC transition being measured is in smaller scale segmental mobility, which occurs at lower temperatures [51, 52]. In addition, the peak height of $\tan\delta$ decreases in the nanocomposites compared to pure PLLA due to decreasing in the energy dissipation as a result of elastic GNPs presence.

3.4. Shape memory properties

3.4.1. Thermal-activation

The typical cyclic shape memory test for pure PLLA and PLLA-GNP1 are plotted in Figure 5 which shows temperature and strain as a function of time.

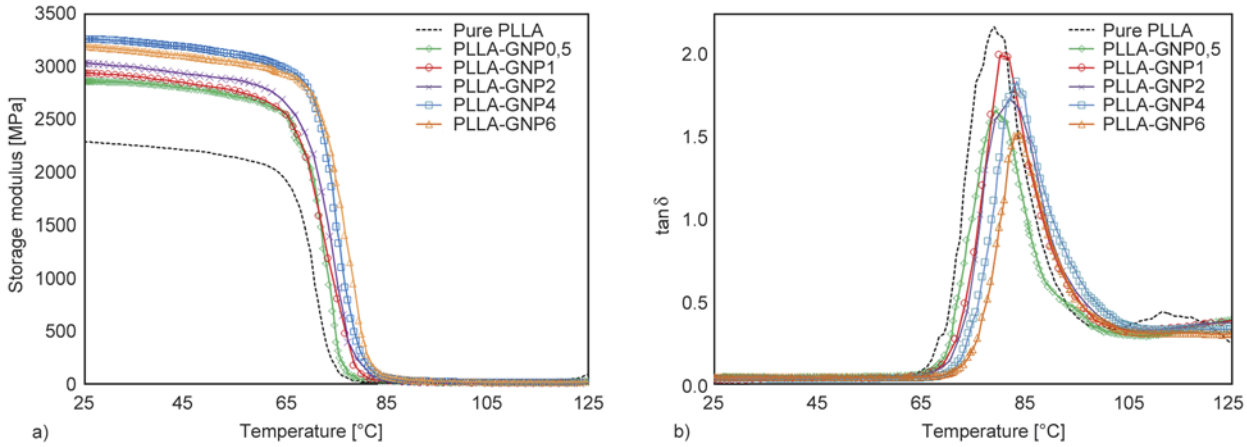

Figure 4. Temperature dependence of (a) storage modulus (E') and (b) loss factor ($\tan\delta$) of pure PLLA and its nanocomposites with GNPs

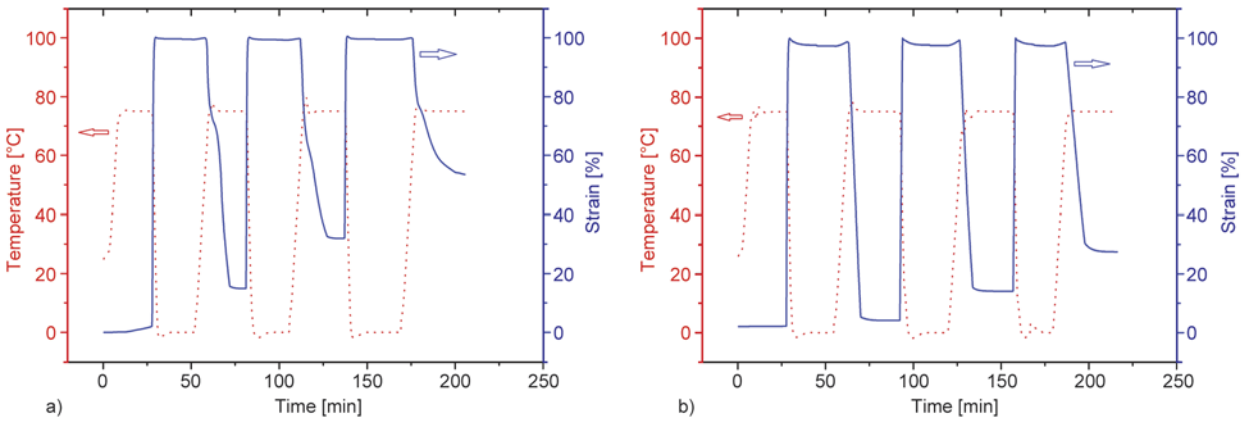

Figure 5. Shape memory cycle of (a) pure PLLA and (b) PLLA-GNP1 utilized with DMA instrument

Detailed shape memory parameters including shape fixity (R_f), shape recovery (R_r) and stress at maximum deformation derived from the plots are presented in Table 2. As can be observed, R_f and R_r of pure PLLA at the first cycle are 98.3 and 85% respectively. The shape memory effect of PLLA is associated to the crystalline and amorphous phase of PLLA acting as fixed and reversible phase respectively [24, 53]. The stress at maximum deformation is higher for nanocomposites compared to pure PLLA due to the enhancing effect of GNPs in the mechanical properties of nanocomposites already mentioned. Figure 6 shows the shape recovery and shape fixity of samples as a function of graphene content. By incorporating of graphene into PLLA, its shape memory properties increases and reaches to optimum at the PLLA-GNP1 then starts reduction at the higher contents of graphene. However, nearly all nanocomposites exhibited higher shape fixity and shape recovery compared to pure PLLA. This may be attributed to the enhancement of crystallinity and thermomechanical properties of nanocomposites resulting in more stable fixing phase leading to better fixation and recovery. Meanwhile, graphene improves heat conductivity which results in more efficient heat transfer during cooling and heating processes leading to faster response with less dissipation of energy and higher values of shape fixity and shape recovery in the nanocomposites.

Table 2. Shape memory properties of pure PLLA and its composites with GNPs actuated by thermal heating at 100% deformation strain

Cycle no.	$\varepsilon_p(N)^*$ [%]	$R_r(N)^{**}$ [%]	$R_f(N)^{***}$ [%]	Stress at max. deformation strain [MPa]
Pure PLLA				
1	14	85±3	98.3	1.0
2	25	80±2	98.2	0.8
3	34	71±1	98.0	0.7
PLLA-GNP0.5				
1	8	91±3	99.2	1.6
2	19	84±2	99.1	1.5
3	30	76±1	98.6	1.3
PLLA-GNP1				
1	2	97±2	99.1	1.7
2	11	89±3	99.0	1.6
3	21	84±2	99.0	1.5
PLLA-GNP2				
1	9	90±3	99.3	1.7
2	20	84±2	99.2	1.4
3	29	78±2	99.1	1.3
PLLA-GNP4				
1	9.1	90±2	99.4	1.7
2	21.1	83±3	99.2	1.3
3	31.0	76±3	99.1	1.2
PLLA-GNP6				
1	11.3	88±2	99.4	1.6
2	23.4	81±2	99.1	1.3
3	32.6	74±3	99.0	1.1

*$\varepsilon_p(N)$ is the unrecovered strain at the N^{th} cycle after heating the sample to T_H temperature
**$R_r(N)$ is the shape recovery rate at the N_{th} cycle
***$R_f(N)$ is the shape fixity rate at the N^{th} cycle

As it is well known [21] the crystalline part of PLLA polymer has more effect on shape memory properties than the amorphous phase, so decreasing trend of shape memory parameters for composites beyond 1 wt% graphene can be attributed to the occurrence of aggregates (Figure 1b) and crystallinity reduction leading to weakening of fixed phase and lowering shape memory performance. With increasing cycle number in the shape memory test, R_r shows decreasing trend due to irreversible processes such as slippage of crystalline domains, plastic deformation of PLLA chains, breaking down of some physical linkage and other factors which cannot be

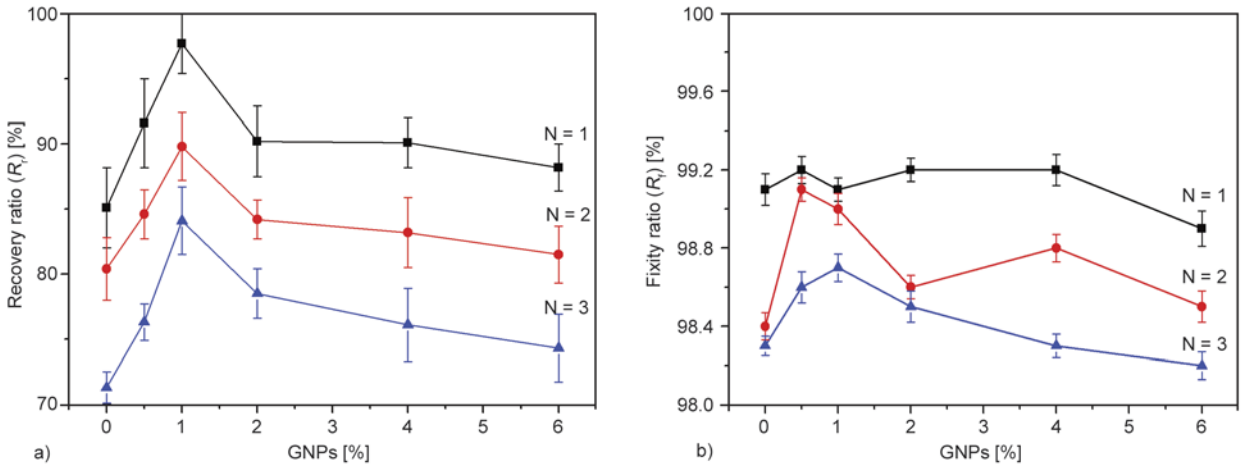

Figure 6. (a) Recovery ratio and (b) fixity ratio relationship versus %GNPs of thermo-activated PLLA nanocomposites; *N* indicates cycle number

recovered during recovery process and result in decreasing R_r. The reduction of R_f may also be correlated to the deformation and displacement of crystalline phase which acts as the fixing part.

3.4.2. Infrared activation

Figure 7 illustrates the thermo-camera images of a free recovery process in the pure PLLA, PLLA-GNP1 and PLLA-GNP6 composites actuated by infrared radiation. The infrared absorption of pure PLLA was low as did not start recovering after 25 s. Graphene enhanced IR absorption of PLLA remarkably which resulted in faster and higher recovery of original shape. The recovering is through transforming infrared light into heat and increasing temperature to switching temperature. As can be seen, at t = 20 s, pure PLLA did not start recovering but PLLA-GNP1 and PLLA-GNP6 recovered around 50 and 90% respectively. The PLLA-GNPs specimens with higher GNPs loadings exhibited faster recovery with lower induction time. This is because more infrared energy is absorbed and transformed into thermal energy within the same radiation time. However, equilibrium recovery which is presented in Table 3 had optimum and reached to maximum (99%) in PLLA-GNP1. This shows that shape recovery of polymers with T_g based switching temperature is accompanied by softening of the glassy

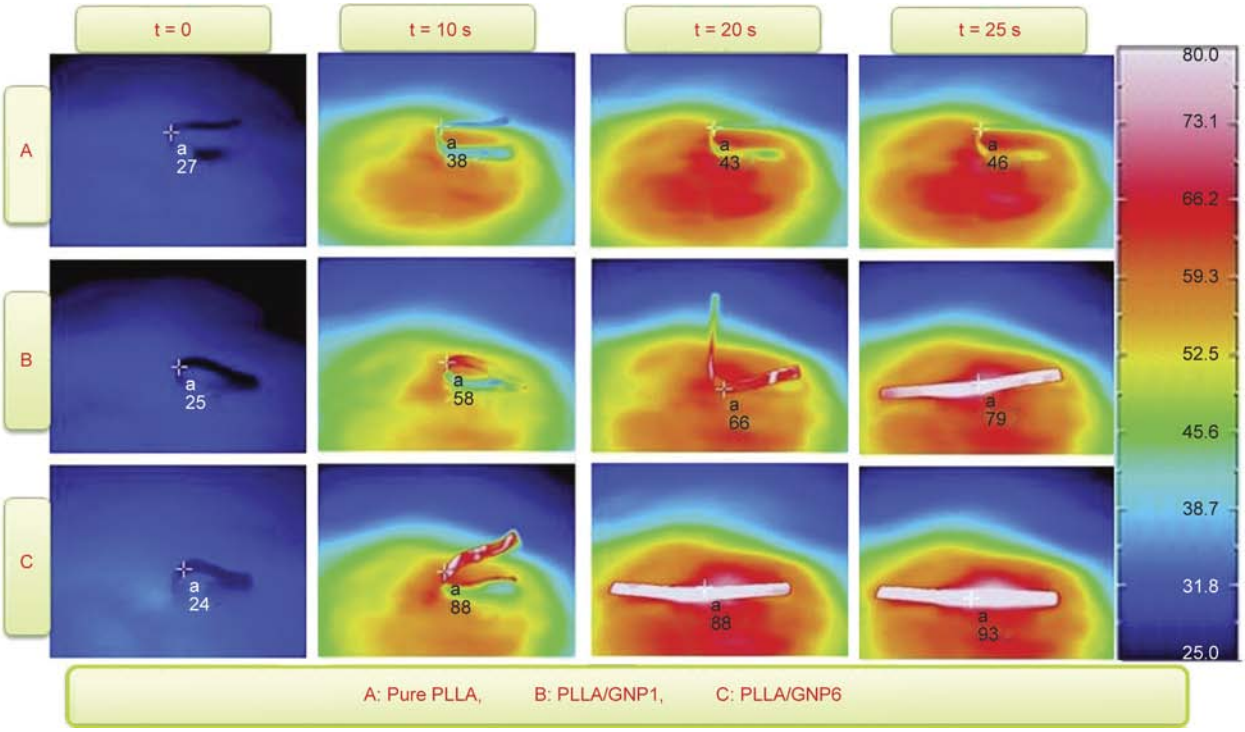

Figure 7. Temperature distribution snapshots of pure PLLA and its nanocomposites during infrared actuation recovery

Table 3. Start time of recovery, equilibrium R_r and max. surface temperature at equilibrium recovery of PLLA/GNPs composites activated by IR

	PLLA	PLLA-GNP0.5	PLLA-GNP1	PLLA-GNP2	PLLA-GNP4	PLLA-GNP6
Start time [s]	154	23	16	14	11	8
Equilibrium R_r [%]	86	98	99	98	94	95
Max. surface temperature at equilibrium recovery	79	86	90	96	103	110

amorphous phase to the rubbery state. This phenomenon is done through energy absorption and chain motion due to entropic elasticity. Although higher GNPs loading helps more energy absorption, but at the same time, it can disturb chain recovery. This should depress shape recovery at graphene loading of higher 2 wt%. The pure PLLA reaches to equilibrium recovery of 86% after 5 min, indicating low infrared absorbability of this polymer.

The maximum surface temperature of samples due to exerting infrared light is shown in Figure 7 and written in Table 3. PLLA may crystallize upon heating over 95°C during infrared heating which would worse its SME remarkably. Therefore, over heating by infrared would be a big concern in the cyclic activation test. To overcome this problem, the light intensity should be adjusted in such a way that leads to not more than 90~95 °C surface temperature increment.

4. Conclusions

In summary, using GNPs in shape memory PLLA enables infrared triggering of shape memory PLLA which is very intriguing in novel applications due to remote control ability of this biodegradable SMP. The effect of GNPs on morphology, crystallinity and thermomechanical properties of PLLA and their correlation to shape memory performance were studied. GNPs had a fine and uniform dispersion in the PLLA matrix at low fractions of GNPs which was resulted in remarkable enhancement of PLLA crystallinity due to nucleating effect of GNPs that was also confirmed by WAXD results. At higher GNPs loading (beyond 2 wt%), the particles started aggregating which was proved by FEG-SEM images and resulted in crystallinity reduction. Thermo-mechanical properties of PLLA were improved by GNPs addition and were leaded to the enhancement of shape memory performance. Recovery ratio of pure PLLA by infrared triggering was only 86% which reached to more than 95% in all of the nanocomposites. Meanwhile, improved mechanical properties of nanocomposites resulted in higher stress deformation of SMPs that is a positive point in SMPs. Finally, compared to pure PLLA, PLLA-graphene nanocomposites showed higher shape memory recovery, stronger recovery stress and quicker response to the stimulus in both activating method.

Acknowledgements

The authors would like to thank Dr. Chiara Ferrari (for thermo-camera photos), Dr. Mauro Zapparoli (for FEG-SEM images) and Dr. Massimo Tonelli (for WAXD analysis) in the CIGS center of University of Modena and Reggio Emillia.

References

[1] Liu C., Qin H., Mather P. T.: Review of progress in shape-memory polymers. Journal of Materials Chemistry, **17**, 1543–1558 (2007). DOI: 10.1039/b615954k

[2] Stylios G. K., Wan T.: Shape memory training for smart fabrics. Transactions of the Institute of Measurement and Control, **29**, 321–336 (2007). DOI: 10.1177/0142331207069479

[3] Hu J.: Shape memory polymers and textiles. Woodhead Publishing Limited, Cambridge (2007).

[4] Sokolowski W., Metcalfe A., Hayashi S., Yahia L., Raymond J.: Medical applications of shape memory polymers. Biomedical Materials, **2**, S23–S27 (2007). DOI: 10.1088/1748-6041/2/1/S04

[5] Maitland D., Benett W. J., Bearinger J. P., Wilson T. S., Small W., Schumann D. L., Jensen W. A., Ortega J. M., Marion J. E., Loge J. M.: Shape memory polymer medical device. U.S. Patent 7744604 B2, USA (2010).

[6] Morshedian J., Khonakdar H. A., Rasouli S.: Modeling of shape memory induction and recovery in heat-shrinkable polymers. Macromolecular Theory and Simulations, **14**, 428–434 (2005). DOI: 10.1002/mats.200400108

[7] Kolesov I., Dolynchuk O., Radusch H-J.: Shape-memory behavior of cross-linked semi-crystalline polymers and their blends. Express Polymer Letters, **9**, 255–276 (2015). DOI: 10.3144/expresspolymlett.2015.24

[8] Raja M., Ryu S. H., Shanmugharaj A. M.: Thermal, mechanical and electroactive shape memory properties of polyurethane (PU)/poly(lactic acid) (PLA)/CNT nanocomposites. European Polymer Journal, **49**, 3492–3500 (2013). DOI: 10.1016/j.eurpolymj.2013.08.009

[9] Leng J., Lan X., Liu Y., Du S.: Shape-memory polymers and their composites: Stimulus methods and applications. Progress in Materials Science, **56**, 1077–1135 (2011).
DOI: 10.1016/j.pmatsci.2011.03.001

[10] Xie T.: Recent advances in polymer shape memory. Polymer, **52**, 4985–5000 (2011).
DOI: 10.1016/j.polymer.2011.08.003

[11] Hu J., Zhu Y., Huang H., Lu J.: Recent advances in shape–memory polymers: Structure, mechanism, functionality, modeling and applications. Progress in Polymer Science, **37**, 1720–1763 (2012).
DOI: 10.1016/j.progpolymsci.2012.06.001

[12] Huang W. M., Zhao Y., Wang C. C., Ding Z., Purnawali H., Tang C., Zhang J. L.: Thermo/chemo-responsive shape memory effect in polymers: A sketch of working mechanisms, fundamentals and optimization. Journal of Polymer Research, **19**, 9952/1–9952/34 (2012).
DOI: 10.1007/s10965-012-9952-z

[13] Wang C. C., Huang W. M., Ding Z., Zhao Y., Purnawali H.: Cooling-/water-responsive shape memory hybrids. Composites Science and Technology, **72**, 1178–1182 (2012).
DOI: 10.1016/j.compscitech.2012.03.027

[14] Lu H., Liu Y., Gou J., Leng J., Du S.: Electroactive shape-memory polymer nanocomposites incorporating carbon nanofiber paper. International Journal of Smart and Nano Materials, **1**, 2–12 (2010).
DOI: 10.1080/19475411003612749

[15] Buckley P. R., McKinley G. H., Wilson T. S., Small W., Benett W. J., Bearinger J. P., McElfresh M. W., Maitland D. J.: Inductively heated shape memory polymer for the magnetic actuation of medical devices. IEEE Transactions on Biomedical Engineering, **53**, 2075–2083 (2006).
DOI: 10.1109/TBME.2006.877113

[16] Sodhi J. S., Rao I. J.: Modeling the mechanics of light activated shape memory polymers. International Journal of Engineering Science, **48**, 1576–1589 (2010).
DOI: 10.1016/j.ijengsci.2010.05.003

[17] Park J. H., Kim B. K.: Infrared light actuated shape memory effects in crystalline polyurethane/graphene chemical hybrids. Smart Materials and Structures, **23**, 025038/1–025038/7 (2014).
DOI: 10.1088/0964-1726/23/2/025038

[18] Paakinaho K., Heino H., Pelto M., Hannula M., Törmälä P., Kellomäki M.: Programmed water-induced shape-memory of bioabsorbable poly(D,L-lactide): Activation and properties in physiological temperature. Journal of Materials Science: Materials in Medicine, **23**, 613–621 (2012).
DOI: 10.1007/s10856-011-4538-6

[19] Huang W. M., Song C. L., Fu Y. Q., Wang C. C., Zhao Y., Purnawali H., Lu H. B., Tang C., Ding Z., Zhang J. L.: Shaping tissue with shape memory materials. Advanced Drug Delivery Reviews, **65**, 515–535 (2013).
DOI: 10.1016/j.addr.2012.06.004

[20] Karger-Kocsis J., Kéki S.: Biodegradable polyester-based shape memory polymers: Concepts of (supra) molecular architecturing. Express Polymer Letters, **8**, 397–412 (2014).
DOI: 10.3144/expresspolymlett.2014.44

[21] Nabipour Chakoli A., Sui J., Amirian M., Cai W.: Crystallinity of biodegradable polymers reinforced with functionalized carbon nanotubes. Journal of Polymer Research, **18**, 1249–1259 (2011).
DOI: 10.1007/s10965-010-9527-9

[22] Zhang X., Lu X., Wang Z., Wang J., Sun Z.: Biodegradable shape memory nanocomposites with thermal and magnetic field responsiveness. Journal of Biomaterials Science, Polymer Edition, **24**, 1057–1070 (2013).
DOI: 10.1080/09205063.2012.735098

[23] Lu X. L., Cai W., Gao Z., Tang W. J.: Shape memory effects of poly(L-lactide) and its copolymer with poly (ε-caprolactone). Polymer Bulletin, **58**, 381–391 (2007).
DOI: 10.1007/s00289-006-0680-6

[24] Meng Q., Hu J., Ho K., Ji F., Chen S.: The shape memory properties of biodegradable chitosan/poly(L-lactide) composites. Journal of Polymers and the Environment, **17**, 212–224 (2009).
DOI: 10.1007/s10924-009-0141-z

[25] Hamad K., Kaseem M., Yang H. W., Deri F., Ko Y. G.: Properties and medical applications of polylactic acid: A review. Express Polymer Letters, **9**, 435–455 (2015).
DOI: 10.3144/expresspolymlett.2015.42

[26] Dong H. Q., Liu L. J., Li Y. Y.: Shape-memory behavior of poly(L-lactide)/poly(ε-caprolactone) blends. Advanced Materials Research, **226**, 171–174 (2011).
DOI: 10.4028/www.scientific.net/AMR.266.171

[27] Ghobadi E., Heuchel M., Kratz K., Lendlein A.: Influence of the addition of water to amorphous switching domains on the simulated shape-memory properties of poly(L-lactide). Polymer, **54**, 4204–4211 (2013).
DOI: 10.1016/j.polymer.2013.05.064

[28] Yan B., Gu S., Zhang Y.: Polylactide-based thermoplastic shape memory polymer nanocomposites. European Polymer Journal, **49**, 366–378 (2013).
DOI: 10.1016/j.eurpolymj.2012.09.026

[29] Lu X., Cai W., Zhao L.: Study on the shape memory behavior of poly(L-Lactide). Materials Science Forum, **475–479**, 2399–2402 (2005).
DOI: 10.4028/www.scientific.net/MSF.475-479.2399

[30] Wong Y. S., Xiong Y., Venkatraman S. S., Boey F. Y. C.: Shape memory in un-cross-linked biodegradable polymers. Journal of Biomaterials Science, Polymer Edition, **19**, 175–191 (2008).
DOI: 10.1163/156856208783432516

[31] Wong Y. S., Venkatraman S. S.: Recovery as a measure of oriented crystalline structure in poly(L-lactide) used as shape memory polymer. Acta Materialia, **58**, 49–58 (2010).
DOI: 10.1016/j.actamat.2009.08.075

[32] Zheng X., Zhou S., Li X., Weng J.: Shape memory properties of poly(D,L-lactide)/hydroxyapatite composites. Biomaterials, **27**, 4288–4295 (2006).
DOI: 10.1016/j.biomaterials.2006.03.043

[33] Paakinaho K., Hukka T. I., Kastinen T., Kellomäki M.: Demonstrating the mechanism and efficacy of water-induced shape memory and the influence of water on the thermal properties of oriented poly(D,L-lactide). Journal of Applied Polymer Science, **130**, 4209–4218 (2013).
DOI: 10.1002/app.39513

[34] Zheng X., Zhou S., Xiao Y., Yu X., Li X., Wu P.: Shape memory effect of poly(D,L-lactide)/Fe_3O_4 nanocomposites by inductive heating of magnetite particles. Colloids and Surfaces B: Biointerfaces, **71**, 67–72 (2009).
DOI: 10.1016/j.colsurfb.2009.01.009

[35] Potts J. R., Dreyer D. R., Bielawski C. W., Ruoff R. S.: Graphene-based polymer nanocomposites. Polymer, **52**, 5–25 (2011).
DOI: 10.1016/j.polymer.2010.11.042

[36] Stankovich S., Dikin D. A., Dommett G. H. B., Kohlhaas K. M., Zimney E. J., Stach E. A., Piner R. D., Nguyen S. T., Ruoff R. S.: Graphene-based composite materials. Nature, **442**, 282–286 (2006).
DOI: 10.1038/nature04969

[37] Kashif M., Chang Y-W.: Supramolecular hydrogen-bonded polyolefin elastomer/modified graphene nanocomposites with near infrared responsive shape memory and healing properties. European Polymer Journal, **66**, 273–281 (2015).
DOI: 10.1016/j.eurpolymj.2015.02.007

[38] Feng Y., Qin M., Guo H., Yoshino K., Feng W.: Infrared-actuated recovery of polyurethane filled by reduced graphene oxide/carbon nanotube hybrids with high energy density. ACS Applied Materials and Interfaces, **5**, 10882–10888 (2013).
DOI: 10.1021/am403071k

[39] Tang Z., Kang H., Wei Q., Guo B., Zhang L., Jia D.: Incorporation of graphene into polyester/carbon nanofibers composites for better multi-stimuli responsive shape memory performances. Carbon, **64**, 487–498 (2013).
DOI: 10.1016/j.carbon.2013.07.103

[40] Wang H., Qiu Z.: Crystallization kinetics and morphology of biodegradable poly(L-lactic acid)/graphene oxide nanocomposites: Influences of graphene oxide loading and crystallization temperature. Thermochimica Acta, **527**, 40–46 (2012).
DOI: 10.1016/j.tca.2011.10.004

[41] Wang H., Qiu Z.: Crystallization behaviors of poly(L-lactic acid)/graphene oxide nanocomposites from the amorphous state. Thermochimica Acta, **526**, 229–236 (2011).
DOI: 10.1016/j.tca.2011.10.006

[42] Sabzi M., Jiang L., Liu F., Ghasemi I., Atai M.: Graphene nanoplatelets as poly(lactic acid) modifier: Linear rheological behavior and electrical conductivity. Journal of Materials Chemistry A, **1**, 8253–8261 (2013).
DOI: 10.1039/c3ta11021d

[43] Norazlina H., Kamal Y.: Graphene modifications in polylactic acid nanocomposites: A review. Polymer Bulletin, **72**, 931–961 (2015).
DOI: 10.1007/s00289-015-1308-5

[44] Murariu M., Dechief A. L., Bonnaud L., Paint Y., Gallos A., Fontaine G., Bourbigot S., Dubois P.: The production and properties of polylactide composites filled with expanded graphite. Polymer Degradation and Stability, **95**, 889–900 (2010).
DOI: 10.1016/j.polymdegradstab.2009.12.019

[45] Garlotta D.: A literature review of poly(lactic acid). Journal of Polymers and the Environment, **9**, 63–84 (2002).
DOI: 10.1023/a:1020200822435

[46] Lendlein A.: Characterization methods for shape-memory polymers. in 'Shape-memory polymer' (eds.: Wagermaier W., Kratz K., Heuchel M., Lendlein A.) Springer, Berlin, Vol 226, 97–145 (2010).

[47] Tobushi H., Hayashi S., Hoshio K., Makino Y., Miwa N.: Bending actuation characteristics of shape memory composite with SMA and SMP. Journal of Intelligent Material Systems and Structures, **17**, 1075–1081 (2006).
DOI: 10.1177/1045389x06064885

[48] Leng J., Wu X., Liu Y.: Infrared light-active shape memory polymer filled with nanocarbon particles. Journal of Applied Polymer Science, **114**, 2455–2460 (2009).
DOI: 10.1002/app.30724

[49] Huang H-D., Ren P-G., Xu J-Z., Xu L., Zhong G-J., Hsiao B. S., Li Z-M.: Improved barrier properties of poly(lactic acid) with randomly dispersed graphene oxide nanosheets. Journal of Membrane Science, **464**, 110–118 (2014).
DOI: 10.1016/j.memsci.2014.04.009

[50] Yu K., Liu Y., Leng J.: Shape memory polymer/CNT composites and their microwave induced shape memory behaviors. RSC Advances, **4**, 2961–2968 (2014).
DOI: 10.1039/c3ra43258k

[51] Xu J., Shi W., Pang W.: Synthesis and shape memory effects of Si–O–Si cross-linked hybrid polyurethanes. Polymer, **47**, 457–465 (2006).
DOI: 10.1016/j.polymer.2005.11.035

[52] Wunderlich B.: Basics of thermal analysis. in 'Thermal analysis of polymeric materials' (ed.: Wunderlich B.) Springer, Berlin, 71–188 (2005).

[53] Lu X. L., Sun Z. J., Cai W., Gao Z. Y.: Study on the shape memory effects of poly(L-lactide-*co*-ε-caprolactone) biodegradable polymers. Journal of Materials Science: Materials in Medicine, **19**, 395–399 (2008).
DOI: 10.1007/s10856-006-0100-3